Chiral Luttinger liquids in graphene tuned by irradiation

Sourav Biswas,[1] Tridev Mishra,[2] Sumathi Rao,[3] and Arijit Kundu[1]
[1]*Department of Physics, Indian Institute of Technology - Kanpur, Kanpur 208 016, India*
[2]*Institute for Theoretical Physics, Georg-August-Universität Göttingen, Friedrich-Hund-Platz 1, 37077 Göttingen, Germany*
[3]*Harish-Chandra Research Institute, HBNI, Chhatnag Road, Jhusi, Allahabad 211 019, India*

(Received 5 April 2020; revised 3 August 2020; accepted 24 September 2020; published 27 October 2020)

We show that chiral co-propagating Luttinger liquid edge modes can be created and tuned by shining high-frequency, (time-reversal breaking) circularly polarized light, normal to the layers. The one-dimensional chiral modes can be localized either at the edge of the system or at a domain-wall created when different portions of the graphene sheet are irradiated by oppositely polarized light; the number of such modes depends on the mismatch of Chern numbers across the boundary or domain wall. These modes, under a high-frequency drive, essentially have a static charge distribution and form a chiral Luttinger liquid under Coulomb interaction, which can be tuned by means of the driving parameters. We also note that unlike the Luttinger liquids created by electrostatic confinement in bilayer graphene, here there is no back-scattering, and hence our wires along the edge or domain wall are stable to disorder.

DOI: 10.1103/PhysRevB.102.155428

I. INTRODUCTION

One of the main reasons for the intense interest in bilayer graphene in recent years has been the fact that it has a tunable band gap [1–5], which can be modulated by an applied gate voltage, unlike the single layer case [6], which typically require staggered fields to open up a gap. More recently, it has been realized that it is possible to confine electrons in gated bilayer structures by applying inhomogeneous electric fields [7] in such a way that one dimensional states can be formed at the domain walls separating the two different insulating regions with different gate voltages. These states are similar to the zero modes that form at domain walls in polyacetyline [8], superconducting vortices [9] or other solitons in field theories [10]. They are free to move in the direction perpendicular to their confinement and are hence nanowires which can be tuned by the gate voltages. The effect of electron-electron interactions on such wires have also been studied [11] and it has been demonstrated that these one-dimensional nanowires behave like strongly interacting Luttinger liquids. Thus bilayer graphene has been shown to be a useful substrate to create and manipulate strongly interacting one-dimensional quantum wires.

Floquet engineering [12–19] or the generation of new Hamiltonians that are not present in static systems but emerge in driven systems, have recently become a very important field of study. In the case of graphene, it has been realized that the possibility of tuning the band gap by shining light greatly increases the potential of applications and there has been considerable work [20–29] on new topological phases obtained by shining light on graphene, as well as bilayer graphene [30–33]. Recent experimental observation of anomalous Hall effect in irradiated graphene confirms the Floquet bands and their nontrivial Berry curvature [34]. Since shining light changes the electric field acting on the electrons in graphene or bilayer graphene, a natural question to ask is whether it would be possible to create confinement of electrons using inhomogeneous light instead of an inhomogeneous electric field using gates. As we shall see in this paper, this question can be answered positively. Moreover, unlike externally applied voltages, shining light breaks the time reversal invariance of the system, and so we find that the edge states that are created by confinement by light are chiral in nature.

Our main focus in this paper will be the edge modes of either single-layer (SLG) or *A-B* stacked bilayer graphene (BLG), which is irradiated by circularly polarized lights (CPL) applied perpendicular to the plane of the layers. Apart from the edge modes at the boundary of such uniformly irradiated systems, confined modes can also emerge at the interface where there is a change in the polarization or phase of the CPL, either on SLG or BLG. We shall show that the steady-state edge modes near each of the valleys turn out to be chiral (either both left-handed or both right-handed), since they result from the breaking of time reversal symmetry by light. For high-frequency driving, these modes are time-independent and in the presence of Coulomb interaction, the interactions between the modes are also essentially time-independent. We shall then show that Coulomb interaction between these chiral modes leads to their mixing, which can then be rediagonalized using the standard techniques of bosonization and Luttinger liquids. We can then obtain the power-law behavior of the charge density and spin density correlation functions and show that the exponents, which should be sensitive to scanning tunneling measurements, can be tuned by changing the amplitude of the impinging radiation. Although we model our system based on single or bilayer graphene, we expect the qualitative aspects of the resulting chiral Luttinger liquid physics to be model independent and hence, a similar

treatment could also work for other topological edge modes of driven symmetry-broken phases.

The paper is organized in the following way. We review the effect of periodic driving in single and bilayer graphene and the topological origin of the edge modes in Sec. II. In Sec. III, we discuss properties of such edge modes, especially their time dependence, when the driving is weak and at high frequency. In Sec. IV, we present the formal Luttinger liquid analysis for interacting edge modes, focusing on the cases of the edge modes of uniformly driven SLG and BLG as well as the domain-wall states of differently driven SLG and BLG. We summarize our findings in Sec. V.

II. IRRADIATION BY CPL: HIGH-FREQUENCY APPROXIMATION

We consider the model of bilayer graphene below and analyze the resulting effective static Hamiltonian in the high-frequency limit. The results of a single-layer of graphene can be recovered in the absence of interlayer hoppings. The Hamiltonian, for the electrons of each spin, on bilayer graphene contains the Hamiltonian of each of the single layers, $H_{\rm SLG}$, and a coupling Hamiltonian between the layers, $H_{\rm inter}$:

$$H_{\rm SLG} = -t \sum_{\langle ij\rangle, l} a^{\dagger}_{l,i} b_{l,j} + \text{H.c.}, \tag{1}$$

$$H_{\rm inter} = t_p \sum_{i\in A,\, j\in B} a^{\dagger}_{2,i} b_{1,j} + \text{H.c.}, \tag{2}$$

where $l = 1, 2$ denotes the layer index, and $a^{\dagger}$ and $b^{\dagger}$ are, respectively, the creation operators for the A and B sublattices of each of the layers. t and t_p are, respectively, the intra- and interlayer hopping amplitudes and we take the estimation $t_p = 0.1t$ with $t = 2.7$ eV. The notation $\langle \dots \rangle$ denotes nearest neighbors. For each single layer, if not coupled to a second layer, the electrons follow a relativistic dispersion near the two distinct Dirac nodes K and K' with the Fermi velocity v given by $\hbar v = \frac{3}{2} t a_0$, where a_0 is the lattice constant. For the rest of the paper we set $\hbar = a_0 = 1$, which serves as our unit of energy and length, respectively. We consider Bernal stacking of the two layers, where the interlayer hopping amplitudes are only between the A sublattice of the top layer (layer 2) and the B sublattice of the bottom layer (layer 1), as shown in the Fig. 1, which is the most stable configuration of bilayer graphene structure [35].

The low-energy Hamiltonian, at a single Dirac node is given by [1,7]

$$H = \begin{pmatrix} 0 & v\pi^{\dagger} & 0 & 0 \\ v\pi & 0 & t_p & 0 \\ 0 & t_p & 0 & v\pi^{\dagger} \\ 0 & 0 & v\pi & 0 \end{pmatrix}, \tag{3}$$

written in the basis of the wave functions $\Psi = (\psi_{A1}, \psi_{B1}, \psi_{A2}, \psi_{B2})$. The canonical momenta are defined as $\pi = p_x + ip_y$, $\pi^{\dagger} = p_x - ip_y$, in terms of the quasimomentum operators p_x and p_y.

We now apply high-frequency circularly polarized light (CPL) perpendicular to the plane of the layers. The vector potential of the radiation is of the form

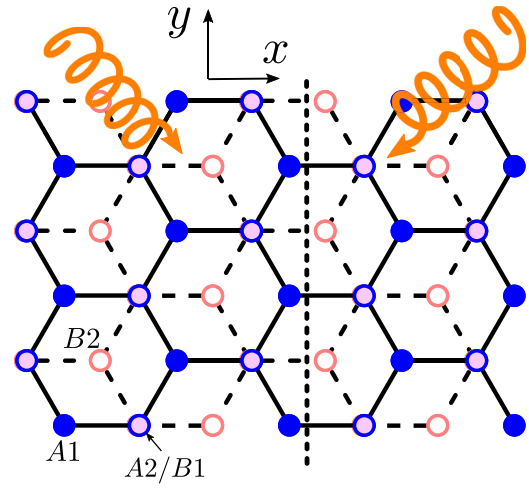

FIG. 1. The primary setup of our study: an A/B stacked bilayer graphene nanoribbon (with a finite width in the x direction) is being irradiated with circularly polarized light of opposite polarizations across a boundary (marked with a dashed line).

$$\mathbf{A}(t) = (A_x \cos(\omega t), A_y \sin(\omega t + \theta), 0), \tag{4}$$

where ω is the frequency of the light and θ is its polarization angle. To work legitimately in the low-energy sector around a single Dirac node, post the application of radiation, we need to assume that the amplitudes A_x and A_y are weak enough to allow for a linear dispersion approximation to hold. The Hamiltonian for BLG in the presence of such a driving force is given by

$$\mathcal{H}(t) = \begin{pmatrix} 0 & v\tilde{\pi}^{\dagger}(t) & 0 & 0 \\ v\tilde{\pi}(t) & 0 & t_p & 0 \\ 0 & t_p & 0 & v\tilde{\pi}^{\dagger}(t) \\ 0 & 0 & v\tilde{\pi}(t) & 0 \end{pmatrix}, \tag{5}$$

where

$$\tilde{\pi}(t) = (p_x - eA_x \cos(\omega t)) + i(p_y - eA_y \sin(\omega t + \theta))$$

denotes the canonical momentum with the gauge field $\mathbf{A}(t)$ being included in $\mathcal{H}$ in a minimally coupled fashion, with e being the electronic charge and setting the speed of light $c = 1$. Since we take the frequency of the light to be very high, i.e., much larger than all other scales (such as intralayer or interlayer hoppings) in the problem, it is possible to compute an effective time-independent Hamiltonian for the system. There are several high-frequency approximations [25,36–41] that one can use to obtain the static Hamiltonian, all of which agree to first order in the inverse frequency $1/\omega$. Using one such approximation, we obtain the effective static Hamiltonian, given by

$$H_{\rm eff} \approx \mathcal{H}_0 + \frac{1}{\omega} \sum_{n=1}^{\infty} \frac{[\mathcal{H}_n, \mathcal{H}_{-n}]}{n} + \mathcal{O}(\omega^{-2}). \tag{6}$$

Here, $\mathcal{H}_n$ denote the Fourier coefficients of the periodic time-dependent Hamiltonian [$\mathcal{H}(t)$ in Eq. (5) in our case] and [,] denotes a commutator bracket. Rewriting the Hamiltonian

$\mathcal{H}(t)$ in Eq. (5) as

$$\mathcal{H}(t) = \mathcal{H}_0 + \mathcal{H}_1 e^{i\omega t} + \mathcal{H}_{-1} e^{-i\omega t},$$

we obtain

$$\mathcal{H}_0 = \begin{pmatrix} 0 & v\pi^\dagger & 0 & 0 \\ v\pi & 0 & t_p & 0 \\ 0 & t_p & 0 & v\pi^\dagger \\ 0 & 0 & v\pi & 0 \end{pmatrix}$$

and the Fourier coefficients $\mathcal{H}_{n=\pm1}$ as

$$\mathcal{H}_{\pm1} = \begin{pmatrix} 0 & -\frac{\lambda}{2}(A_x \mp A_y e^{\pm i\theta}) & 0 & 0 \\ -\frac{\lambda}{2}(A_x \pm A_y e^{\pm i\theta}) & 0 & 0 & 0 \\ 0 & 0 & 0 & -\frac{\lambda}{2}(A_x \mp A_y e^{\pm i\theta}) \\ 0 & 0 & -\frac{\lambda}{2}(A_x \pm A_y e^{\pm i\theta}) & 0 \end{pmatrix},$$

where $\lambda = ve$. The effective time-independent Hamiltonian for the BLG system driven by high-frequency CPL is thus obtained from Eq. (6) (restricting $n \leqslant 1$), up to order $1/\omega$, as

$$H_{\text{eff}} = \begin{pmatrix} -\frac{\lambda^2\gamma}{4\omega}\cos\theta & v\pi^\dagger & 0 & 0 \\ v\pi & \frac{\lambda^2\gamma}{4\omega}\cos\theta & t_p & 0 \\ 0 & t_p & -\frac{\lambda^2\gamma}{4\omega}\cos\theta & v\pi^\dagger \\ 0 & 0 & v\pi & \frac{\lambda^2\gamma}{4\omega}\cos\theta \end{pmatrix}, \tag{7}$$

where $\gamma = 4A_xA_y$. Hence, the effect of the CPL, in the high-frequency limit, is essentially to introduce an on-site modulation on the sublattice sites of the two layers. This amounts to a sublattice staggered potential at the A and B sites of both layers. Thus we see that shining light gives rise to an effective Haldane gap at both the valleys.

In the above effective Hamiltonian, if we set $t_p = 0$, we recover the effective Hamiltonian for each of the single layers of the graphene sheet as

$$H_{\text{eff}}^{\text{SLG}} = \begin{pmatrix} -\frac{\lambda^2\gamma}{4\omega}\cos\theta & v\pi^\dagger \\ v\pi & \frac{\lambda^2\gamma}{4\omega}\cos\theta \end{pmatrix}, \tag{8}$$

which has the form of a two-dimensional Dirac equation with the mass term given by $m = \frac{\lambda^2\gamma}{4\omega}\cos\theta$. This immediately implies that the sign of the mass term, and thus the Chern number can be modified by changing the sign of $\cos\theta$, near each of the Dirac points. If we have opposite polarization of the irradiation for $x > 0$ and $x < 0$, then this gives rise to two resulting topological edge modes at $x = 0$, of the same chirality, one each near momenta K and K'.

For BLG with $t_p \neq 0$, our next step is to compute the effective low-energy two band model which describes the physics from the four-band Hamiltonian (7) using a prescription [42] similar to that which has been used for gated bilayer graphene [7]. To do that, we first rewrite the H_{eff} in a modified site basis $(A1, B2, B1, A2)$ where the effective Hamiltonian takes the form

$$H_{\text{eff}} = \begin{pmatrix} -\frac{\lambda^2\gamma}{4\omega}\cos\theta & 0 & v\pi^\dagger & 0 \\ 0 & \frac{\lambda^2\gamma}{4\omega}\cos\theta & 0 & v\pi \\ v\pi & 0 & \frac{\lambda^2\gamma}{4\omega}\cos\theta & t_p \\ 0 & v\pi^\dagger & t_p & -\frac{\lambda^2\gamma}{4\omega}\cos\theta \end{pmatrix} \equiv \begin{pmatrix} H_{11} & H_{12} \\ H_{21} & H_{22} \end{pmatrix}, \tag{9}$$

where H_{ij} denote the appropriate 2×2 blocks. The eigenvalues ϵ of H_{eff} can then be shown to follow the identity

$$\det(H_{\text{eff}} - \epsilon) = \det(H_{11} - H_{12}(H_{22} - \epsilon)^{-1}H_{21} - \epsilon) \times \det(H_{22} - \epsilon). \tag{10}$$

In the low-energy regime where $\epsilon \ll t_p$ and where $\frac{\lambda^2\gamma}{4\omega} \ll t_p$, since $H_{22} - \epsilon \simeq H_{22}$, we can project the four-band Hamiltonian onto the two low-energy bands, given by the Hamiltonian

$$H_{\text{eff}}^L = H_{11} - H_{12}H_{22}^{-1}H_{21} = \begin{pmatrix} -\frac{\lambda^2\gamma}{4\omega}\cos\theta\left(1 + \frac{v^2p^2}{t_p^2}\right) & -\frac{v^2\pi^{\dagger 2}}{t_p} \\ -\frac{v^2\pi^2}{t_p} & \frac{\lambda^2\gamma}{4\omega}\cos\theta\left(1 + \frac{v^2p^2}{t_p^2}\right) \end{pmatrix}, \tag{11}$$

where $p = (\pi\pi^\dagger)^{\frac{1}{2}} = \sqrt{p_x^2 + p_y^2}$. Under the approximation where we drop the second term in the diagonal part of the Hamiltonian, this Hamiltonian becomes very similar to the Hamiltonian derived for gated bilayer graphene [7]. In this approximation, the potential terms on the diagonal and the momentum dependent terms on the off-diagonal parts of the Hamiltonian are decoupled. Any position dependence in this Hamiltonian can now be introduced in the system consistently by simply promoting p_x and p_y

to their corresponding differential operator representations. This allows the eigenvalue problem to be duplicated by a quasi-classical Hamiltonian of the kind derived in Ref. ([7]), written as

$$\tilde{H}^L_{\text{eff}} = -\phi(x)\sigma_z - \left(p_x^2 - p_y^2\right)\sigma_x - 2p_x p_y \sigma_y, \tag{12}$$

where $\phi(x) = t_p^2 a_0^2/2v^2 \times (\lambda^2\gamma \cos\theta(x)/4\omega)$ in our case and momenta are measured in units of inverse lattice constant (i.e., $1/a_0$). For the case of a bilayer strip, which is finite in the x direction and translationally invariant in y, p_y is a good quantum number, whereas p_x is an operator. Hence, we need to solve the pair of coupled differential equations, obtained from the eigenvalue problem for the Hamiltonian in Eq. (12), for the potential profile contained in $\phi(x)$. When $\phi(x)$ has a step profile, changing sign across a boundary, topological zero-energy modes are localized at the kink. For the case of confined modes, we introduce a position dependence in the polarization angle of the irradiation. The zero modes are then confined at the domain wall obtained when we have light of two different polarizations for $x < 0$ and $x > 0$.

In fact, the Chern number associated with the ground state of Eq. (12) is given by $\text{sgn}(\phi)$, which is easily seen as follows. We rewrite the effective Hamiltonian (12) as

$$\tilde{H}^L_{\text{eff}} \equiv \begin{bmatrix} -\phi & k^2 e^{2i\theta} \\ k^2 e^{-2i\theta} & \phi \end{bmatrix}, \tag{13}$$

with $k = \sqrt{k_y^2 + k_x^2}$ and $\theta = \tan^{-1}(\frac{k_x}{k_y})$. Diagonalization gives the wave functions

$$\Psi_\pm = \begin{bmatrix} e^{i\theta} \frac{k^2}{\sqrt{k^4 + (\phi \pm \sqrt{\phi^2+k^4})^2}} \\ e^{-i\theta} \frac{\phi \pm \sqrt{\phi^2+k^4}}{\sqrt{k^4 + (\phi \pm \sqrt{\phi^2+k^4})^2}} \end{bmatrix} \tag{14}$$

with energies $\epsilon_\pm = \pm\sqrt{\phi^2 + k^4}$. For the lower energy band, the Chern number is then readily given by

$$\frac{i}{2\pi}\int d^2k [\langle \partial_{k_x}\Psi_-|\partial_{k_y}\Psi_-\rangle - \langle \partial_{k_y}\Psi_-|\partial_{k_x}\Psi_-\rangle] = \text{sgn}(\phi). \tag{15}$$

For the edge of the sample, this implies the presence of a single chiral mode for each spin. On the other hand, Chern number changes $\Delta C = 2$, for each spin, across the boundary of regions with different signs of ϕ, i.e., in the case where the two sides are driven with different polarizations $\phi = +\pi$ and $\phi = -\pi$. So there are two chiral modes for each spin at the domain wall.

All of this is at a single Dirac point. At the other Dirac point, the operators π and $\pi^\dagger$ are interchanged. It is easy to check that this only leads to a change in sign in the effective potential term $\phi(x)$ in Eq. (12). So essentially, the operators at the K and K' points are related by the symmetry $\phi(x) \to -\phi(x)$, $p_y \to -p_y$. This, in turn, comes from the fact that the effect of radiation essentially acts like a time-reversal symmetry breaking staggered potential and so, unlike in the gated bilayer graphene system, the edge states at both the K and the K' valleys have the same chirality (decided by the chirality of the circular polarization of the impinging light). In general, for an n-layer graphene sheet, one expects the Chern number change for each boundary of the irradiated region to be $n \times \text{sign}(\phi)$ [43,44], for each spin, and at the domain wall, since it has two "boundaries," the change will be twice as much. The spread of the wave function at the domain wall depends on the driving strength and amplitude. Further, the irradiation with two different polarizations at the two sides may interfere near the domain-wall, giving rise to an unpolarized region, spreading over a width of the order of the wave length, although one expects the edge modes to be robust given their topological origin.

III. TIME-DEPENDENT EDGE MODES

In the previous section, we discussed how the polarized irradiation induces topological gaps at the K and K' Dirac points. If a single layer of bilayer graphene is irradiated uniformly with a circularly polarized light, the resulting topological state results in one and two chiral edge modes, respectively, for single and bilayer, at the boundary of the sample. If the regions irradiated by opposite polarizations are separate, as shown in Fig. 1, one expects edge modes at the interface. If the two sides are irradiated by right and left circularly polarized light (i.e., $\theta = 0, \pi$ on the two sides with $A_x = A_y = A_0$), the net change of Chern number, for each spin, across the interface is two (four) for single-layer (bilayer) graphene and accordingly one expects two (four) chiral modes to run along the interface. We study the edge modes through a tight-binding simulation, by incorporating the vector potential Eq. (4) in the Hamiltonian (1) by Peierls substitution, neglecting the phase difference in $\vec{A}(t)$ between the two layers, which is justified as $l_{\text{int}}\omega/c \ll 1$, where c is the velocity of light and l_{int} is the interlayer distance. The steady states of the time-periodic Hamiltonian $H(t)$ after the Peierls substitution can be found using the Floquet theorem, which states that the eigenstates will be of the form

$$\psi_\alpha(t) = e^{-i\epsilon_\alpha t} u_\alpha(t), \tag{16}$$

where ϵ_αs are the "quasienergies" and $u_\alpha(t)$ are periodic functions, called the Floquet states, both of which can be found from the eigensystem equation

$$(i\partial_t - H(t))u_\alpha(t) = \epsilon_\alpha u_\alpha(t). \tag{17}$$

For a high-frequency drive, the quasienergy spectrum of a nanoribbon is shown in Fig. 2, highlighting the edge modes, for both the case of edge modes at the interface of differently driven regions of SLG and BLG, as well as at the boundary of a uniformly driven BLG. The edge modes appear at each K/K' points with a slightly different Fermi velocity v_1 and v_2. Appendix A has a discussion of how higher orders in the high-frequency expansion lead to the fact that $v_1 \neq v_2$. The spread of these edge modes depends on the topological gap, which is proportional to A_0^2/ω. In Appendix B, we briefly discuss such dependence.

Before we proceed to analyze the properties of the topological edge modes under Coulomb interactions, which we introduce perturbatively, a justification of the use of the non-interacting Floquet analysis is due. A number of recent papers [39,45–47] argue that, for a rapidly driven closed interacting system, the heating timescale (τ_h) is exponentially large in

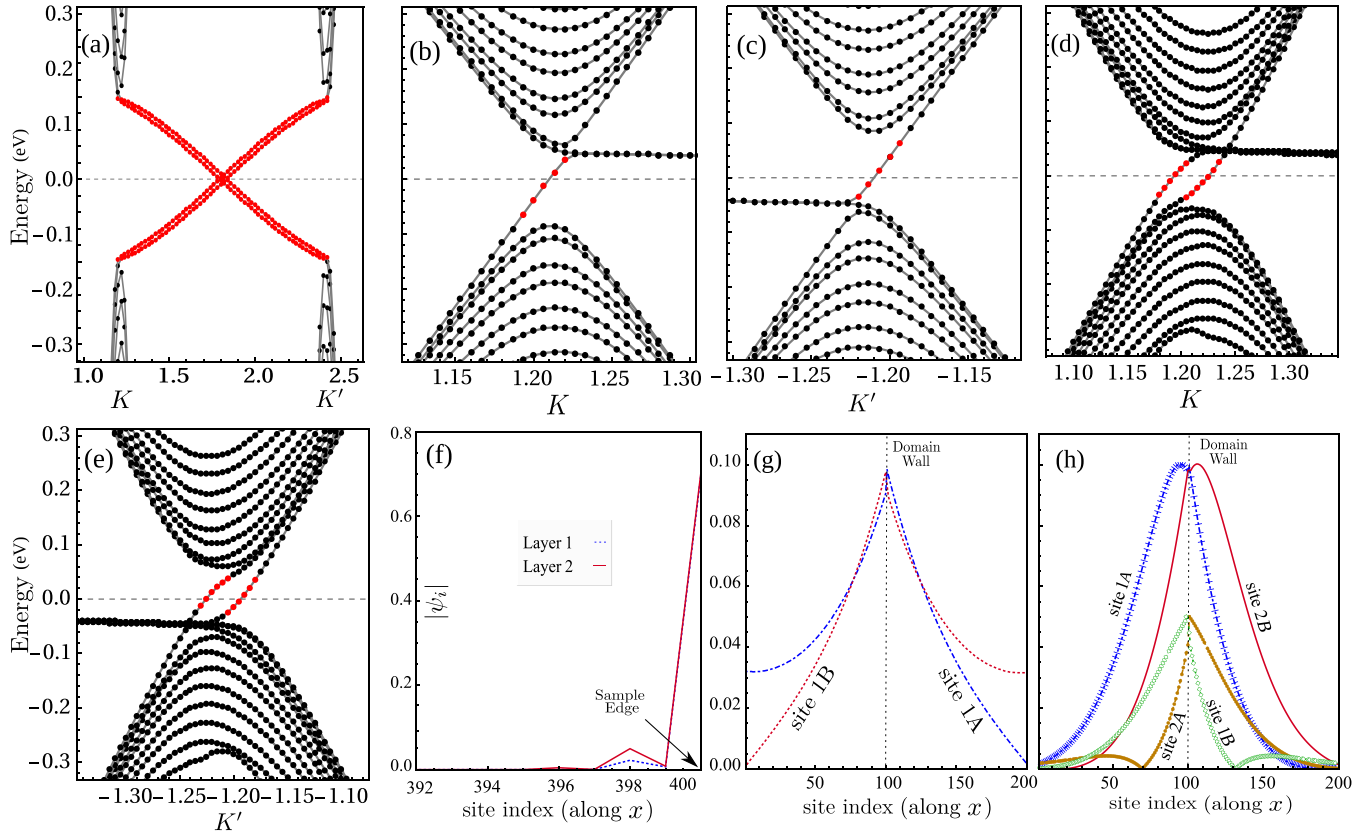

FIG. 2. (a): Quasienergy dispersion and edge modes (marked) for an *uniformly driven* BLG nanoribbon as a function of the momentum along the axis of the ribbon (identical for both the spins). At a given edge only two *chiral* modes are present (see main text for discussion). The result for a uniformly driven SLG is very similar to the case of a uniformly driven BLG, except there is a single mode of each spin at the boundary. (b) and (c) show the quasienergy modes [Eq. (17)] of the SLG nano-ribbon system with *two oppositely polarized irradiation* on two patches, as a function of the momentum along the axis of the ribbon (k_y, see Fig. 1), near the K and K' Dirac points (momentum is measured in units of $1/a_0$, a_0 being the lattice spacing of the hexagonal structure), in a given spin sector. A total of two edge modes, which run along the domain-wall between the differently irradiated regions are marked in the figure. There are also edge modes at the boundary of the sample, running between the valleys, which are shown, but not marked. Similarly, the quasi-energy dispersion and domain-wall modes, with *two oppositely polarized irradiation* on two patches, are shown in (d) and (e) for BLG. For one of the two edge modes in (a), their spatial character is depicted in (f), showing the weight of the steady-state wave functions in layers 1 and 2. For the domain-wall mode in (b), the spatial character is depicted in (g), showing the weight of the steady-state wave functions in A and B sublattices in the single layer 1. For one of the domain-wall modes in (d), the weights of the wave function in shown in (h), in both sublattices as well as in the two layers. The spread of the wave functions in all cases depends on the strength and the frequency of the irradiation as well as on the gap of the bulk-states at the relevant momentum point. A frequency of $\omega/t = 30$, an amplitude of $A_0 = 0.3$, and 200 sites for each layer (each site contains A and B sublattices) has been used in the numerical simulation.

the driving frequency. In the intermediate time, the system's dynamics is governed by an effective Hamiltonian, which one may obtain from a high-frequency approximation, such as the van Vleck expansion used in our system. If our system is weakly connected to an environment, giving rise to a relaxation timescale τ_l, then as long as $\tau_l \ll \tau_h$, one expects the system to not be heated. Further, with a high-frequency drive, even when there is a gap opening due to the breaking of a symmetry, such as in our case, one expects no population inversion [48,49]. This allows us to consider the occupations to have the standard Fermi-Dirac distribution. We further consider that the bulk system, which has Dirac dispersion near the Fermi energy, is essentially noninteracting and that the Coulomb interaction is only important in the edge modes. This assumption, strictly speaking, needs to be further justified, and can be argued as follows. First, since the edge modes are topological, they are expected to be robust against weak interactions in the bulk. Second, since the edge modes are one-dimensional, the effect of Coulomb interaction among them can not be neglected.

Assuming that the preceding approximations hold, we further proceed to make an another argument to justify the application of Luttinger liquid theory, namely, we argue that the interaction among the edge modes are also effectively time-independent. In the presence of perturbative interactions, the effective interaction elements among modes with similar quasienergies can be written as

$$\langle \psi_\alpha(t)|\hat{V}_{\rm int}|\psi_{\alpha'}(t)\rangle = \langle u_\alpha(t)|\hat{V}_{\rm int}|u_{\alpha'}(t)\rangle, \qquad (18)$$

where we have used the fact that $|\epsilon_\alpha - \epsilon_{\alpha'}| \ll \omega$. Expanding in Fourier components, $|u_\alpha(t)\rangle = \sum_n e^{-in\omega t}|u_\alpha^{(n)}\rangle$, the

right-hand side of the above equation can be written as

$$= \sum_{n,m} e^{i(n-m)\omega t} \langle u_\alpha^{(n)} | \hat{V}_{\rm int} | u_{\alpha'}^{(m)} \rangle. \tag{19}$$

We show in Fig. 3 that for the edge modes, $|u_\alpha^{(0)}\rangle$ is dominant, and other Fourier components can be neglected [i.e., the time dependence of $\psi_\alpha(t)$ is governed by only the dynamical phase factor]. This essentially results from the fact that the gap opening (and thus the resulting edge modes) at the K and K' points takes place even for an infinitesimal driving amplitude without any relevant change of the occupation number [48,49]. This allows us to simplify the interaction matrix elements among the edge modes to be effectively time-independent.

As the effective static Hamiltonian can only predict dynamics in stroboscopic times [40], the states may still have significant transverse dynamics. We check this in Fig. 3, where, we examine the transverse dispersion of a wave packet, initially introduced at the domain-wall of the two topologically distinct regions, when driven by the time-periodic Hamiltonian. The results show that, for a few hundred cycles, the wave packet can be considered to be confined at the interface of the two regions, although for BLG (unlike for SLG), the wave packet starts spreading for about a 1000 cycles. In contrast, if the dynamics had been strictly driven by a time-independent effective Hamiltonian, as was derived in the last section, we would have found that the wave packet would have remained confined to the interface for a much longer time. This hints at a nonvanishing transverse velocity and a limit to the timescale for the validity of the effective one-dimensional nature of the low-energy excitations. For a uniformly irradiated sample, we find the wave packet to be even more robust at the edge, when the edge is a zigzag edge, also shown in Fig. 3. This variation of timescales in these different cases can be attributed to the localization lengths of the edge-states which one expects to be much smaller when the bulk gap is larger (depending on the transverse momentum).

It should also be noted that if the original wave packet had been prepared in the state of $|u_\alpha(t)\rangle$ (or, equivalently, $\approx |u_\alpha^{(0)}\rangle$), the wave packet would have been confined to the boundary for an infinite time, as the Floquet states would then be eigenstates of the Hamiltonian. This, however, would require careful initial state preparation, which may not always be an easy task.

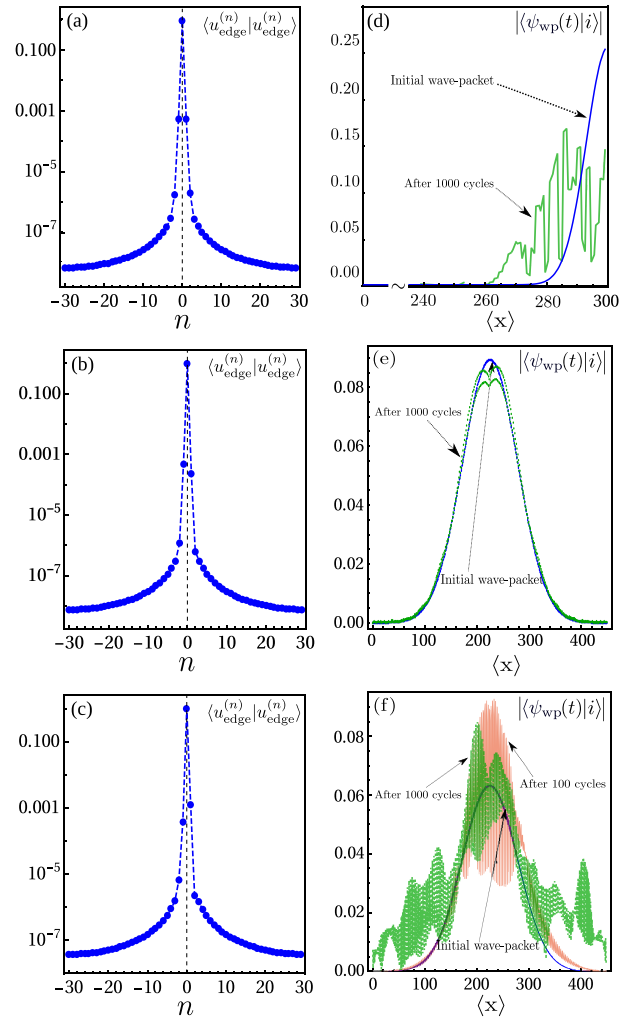

FIG. 3. [(a)–(c)] For one of the edge modes, the weight of the discrete Fourier components of the Floquet states is plotted (in a logarithmic scale), showing that the $n = 0$ component is several orders of magnitude larger than the other components, giving rise to essentially time-independent Floquet modes and allowing for an effective time-independent interaction among them. (a) Corresponds to the edge mode at the boundary of uniformly driven BLG, whereas (b) and (c) correspond to the edge mode at the interface of regions driven with opposite polarization in SLG and BLG respectively. In (d)–(f), we show the dynamics of a Gaussian wave packet (which is not an eigenstate) introduced at the interface of the system with two different polarizations for these corresponding three cases. Even after thousands of cycles, the wave packet remains essentially confined to the edge. In (d), we depict the dynamics at the edge of uniformly driven BLG, where we show an initial Gaussian wave packet and its modification after 1000 cycles of the drive. Similarly, in (e) and (f), we demonstrate the effect when the wave packet is introduced at the interface region in SLG and BLG, respectively, where we show an initial Gaussian wave packet and its modification after 100 as well as 1000 cycles of the drive. The parameters used were $\omega/t = 30$ and $A_0 = 0.3$. The results for the edge of uniformly driven SLG (not shown) is qualitatively similar to that of the BLG.

IV. LUTTINGER LIQUID ANALYSIS

As argued in the previous section, the steady-state edge modes in this system are essentially time-independent, allowing us to consider an effective time-independent interaction Hamiltonian, which is crucial for our use of Luttinger liquid theory [50]. Keeping this in mind, we write the interaction among the (effectively time-independent) edge states of the time-periodic Hamiltonian as

$$H_{\rm int} = \frac{1}{2} \int d\vec{r} d\vec{r}' \hat{\rho}(\vec{r}) V(\vec{r} - \vec{r}') \hat{\rho}(\vec{r}'). \tag{20}$$

Here we assume that $\hat{\rho}(r)$ has a trivial time-dependence, which we justify as follows. We write the field operator of the driven system as $\Psi^\dagger(\vec{r}, t) = \sum_\alpha \langle \vec{r} | \psi_\alpha(t) \rangle a_\alpha^\dagger = \sum_{\alpha,n} e^{i(\epsilon_\alpha + n\omega)t} \langle \vec{r} | u_\alpha^{(n)} \rangle a_\alpha^\dagger$, where $|u_\alpha(t)\rangle = \sum_n e^{-in\omega t} |u_\alpha^{(n)}\rangle$ are

the Floquet states as defined earlier as well. Then,

$$\begin{aligned}\hat{\rho}(\vec{r},t) &= \Psi^{\dagger}(\vec{r},t)\Psi(\vec{r},t)\\ &= \sum_{\alpha,\beta}\sum_{n,m} e^{i(\epsilon_\alpha-\epsilon_\beta)t}\left[e^{i(n-m)\omega t}\left\langle u_\beta^{(m)}\middle|\vec{r}\right\rangle\left\langle\vec{r}\middle|u_\alpha^{(n)}\right\rangle\right]a_\alpha^{\dagger}a_\beta\\ &= \sum_{\alpha,\beta} e^{i(\epsilon_\alpha-\epsilon_\beta)t}\left[\sum_n \left\langle u_\beta^{(n)}\middle|\vec{r}\right\rangle\left\langle\vec{r}\middle|u_\alpha^{(n)}\right\rangle\right]a_\alpha^{\dagger}a_\beta\\ &\quad+\sum_{\alpha,\beta} e^{i(\epsilon_\alpha-\epsilon_\beta)t}\left[\sum_{n,m\neq n} e^{i(n-m)\omega t}\left\langle u_\beta^{(m)}\middle|\vec{r}\right\rangle\left\langle\vec{r}\middle|u_\alpha^{(n)}\right\rangle\right]a_\alpha^{\dagger}a_\beta.\end{aligned} \tag{21}$$

So, if $|\langle\vec{r}|u^{(0)}\rangle| \gg |\langle\vec{r}|u^{(n\neq 0)}\rangle|$ is satisfied, then generally the nontrivial time dependence of the above equation (second part) can be dropped. As mentioned before, we have verified this in Figs. 3(a)–3(c). Further, we have also studied wave packet dynamics of a Gaussian wave packet in Figs. 3(d)–3(f), where we have obtained the timescale below which any transverse motion due to the dynamics of the edge-states can be neglected and a Luttinger liquid formalism based on the time-independent density operator can be justified.

We consider four cases: (i) for a uniformly irradiated sample of SLG, within the effective time-independent description, at low energy, we have a chiral mode of each spin at the edge of the sample. (ii) For a uniformly irradiated sample of BLG, we have two chiral modes (of each spin) at the edge of the sample. (iii) For a sample with two regions irradiated with oppositely polarized light, there is one chiral mode at each of the Dirac points K and K' (in total two), for each spin (σ) for the SLG and (iv) we have two chiral modes at each of the Dirac points K and K' for each spin (σ) for the BLG. When we have multiple modes of each spin, we index these modes by $\alpha = 1, 2$ for the cases (ii) and (iii), and $\alpha = 1_K, 2_K, 1_{K'}, 2_{K'}$ for the case (iv). Assuming translation invariance along the y direction, we can further write the field operator for each mode, taking into account only the modes near the Fermi energy, with $\vec{R} = (x, y)$ as

$$\hat{\Psi}_\sigma(\vec{R}) = \sum_\alpha \hat{\Psi}_{\alpha\sigma}(\vec{R}) = \sum_\alpha \phi_\alpha(x)e^{ik_F^\alpha y}\hat{\xi}_{\alpha\sigma}(y)\,, \tag{22}$$

where $\hat{\xi}_{\alpha\sigma}(y)$ is a slowly varying function along y. The interaction Hamiltonian can then be expressed as

$$\begin{aligned}\tilde{H}_{\rm int} &= \frac{1}{2L_y}\sum_{\sigma\sigma' yy'}\int dy dy'\,\hat{\Psi}_\sigma^{\dagger}(\vec{R})\hat{\Psi}_{\sigma'}^{\dagger}(\vec{R}')V(|\vec{R}-\vec{R}'|)\\ &\quad\times\hat{\Psi}_{\sigma'}(\vec{R}')\hat{\Psi}_\sigma(\vec{R})\,,\\ &\equiv \frac{1}{2}\sum_{\sigma\sigma' yy'\{\alpha\}}\int dy dy'\;\; h,\end{aligned} \tag{23}$$

where the integrand can be written as

$$\begin{aligned}h &= \frac{e^{iy\Delta k - i\bar{y}(k_F^\gamma - k_F^\beta)}}{\sqrt{\bar{y}^2+(x-x')^2}}\phi_\alpha^*(x)\phi_\beta^*(x')\phi_\gamma(x')\phi_\delta(x)\\ &\quad\times\hat{\xi}_{\alpha\sigma}^{\dagger}(y)\hat{\xi}_{\beta\sigma'}^{\dagger}(y-\bar{y})\hat{\xi}_{\gamma\sigma'}(y-\bar{y})\hat{\xi}_{\delta\sigma}(y),\end{aligned} \tag{24}$$

where $\bar{y} = y - y'$ and considering the functions $\hat{\xi}$ to be slowly varying, momentum conservation requires $\Delta k = 0$. Note that we have assumed the potential $V(|\mathbf{R}-\mathbf{R}'|)$ to be of the form $e^2/\sqrt{\bar{y}^2+(x-x')^2}$.

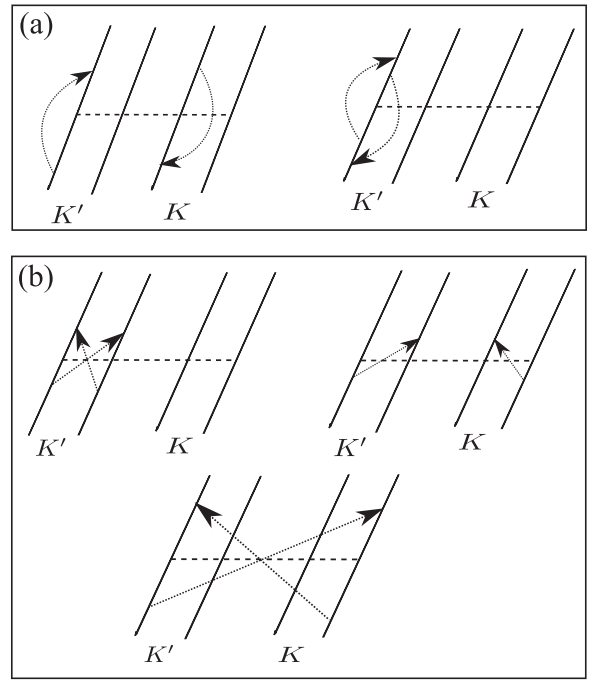

FIG. 4. Various types of scattering processes allowed by the interaction Hamiltonian among the domain-wall modes in BLG. (a) shows the processes which are of the density-density type (class I), whereas (b) shows all the inter-mode scattering processes (class II). The processes in (b) are sub-dominant by several orders of magnitude and are neglected in our analysis. Some of the processes are naturally not possible in case of domain-wall modes in SLG or the edge modes of uniformly driven BLG.

Broadly speaking, the possible scattering processes can be divided into two classes, shown as classes I and II in Fig. 4. Computing the bare scattering amplitudes of all the processes, we find that density-density type interactions (class I) are the dominant ones by several orders of magnitude and hence, we keep only such processes. Furthermore, since all scatterings in class I take place in the same mode, we may take $k_F^\gamma = k_F^\beta$. In this case, the form of h can be written as

$$\begin{aligned}h &= \frac{1}{\sqrt{\bar{y}^2+(x-x')^2}}\phi_\alpha^*(x)\phi_\beta^*(x')\phi_\beta(x')\phi_\alpha(x)\\ &\quad\times\hat{\xi}_{\alpha\sigma}^{\dagger}(y)\hat{\xi}_{\beta\sigma'}^{\dagger}(y-\bar{y})\hat{\xi}_{\beta\sigma'}(y-\bar{y})\hat{\xi}_{\alpha\sigma}(y).\end{aligned} \tag{25}$$

We may now write the one-dimensional form of the interaction Hamiltonian in terms of the standard two-body scattering amplitudes $V_{\alpha\alpha'\alpha'\alpha}$ defined below as

$$\begin{aligned}\tilde{H}_{\rm int} &\approx \frac{\alpha_g}{2}\int dy\sum_{\alpha\alpha'}V_{\alpha\alpha'\alpha'\alpha}\\ &\quad\times\sum_{\sigma\sigma'}\hat{\xi}_{\alpha\sigma}^{\dagger}(y)\hat{\xi}_{\alpha'\sigma'}^{\dagger}(y)\hat{\xi}_{\alpha'\sigma'}(y)\hat{\xi}_{\alpha\sigma}(y),\end{aligned} \tag{26}$$

where the scattering amplitudes are given by

$$\begin{aligned}V_{\alpha\alpha'\alpha'\alpha} &= \sum_{xx'\bar{x}\{\alpha\}}\frac{1}{\sqrt{\bar{y}^2+(x-x')^2}}\\ &\quad\times\phi_\alpha^*(x)\phi_{\alpha'}^*(x')\phi_{\alpha'}(x')\phi_\alpha(x).\end{aligned} \tag{27}$$

These amplitudes can be computed, numerically, from the Floquet states. An effective fine-structure constant $\alpha_g \approx 2$ for single-layer graphene is used, and we write all velocities in terms of the velocity of electrons in graphene. For bosonization, we adopt the following notations: $\hat{\xi}_{\alpha\sigma}(y) \sim e^{-i2\sqrt{\pi}\Phi_{\alpha\sigma}(y)}$; $\rho_{\alpha\sigma}(y) = \hat{\xi}^{\dagger}_{\alpha\sigma}(y)\hat{\xi}_{\alpha\sigma}(y) = -\frac{1}{\sqrt{\pi}}\nabla\Phi_{\alpha\sigma}$. Here $\Phi_{\alpha\sigma}(y)$ is the bosonic field operator. Note that we have not included Klein factors, as they can be set to unity in the density and they do not affect the correlation functions that we compute in this paper. In this notation, the density-density interaction becomes

$$\rho_{\alpha\sigma}\rho_{\alpha'\sigma'} = \frac{1}{\pi}\nabla\Phi_{\alpha\sigma}(y)\nabla\Phi_{\alpha'\sigma'}(y). \tag{28}$$

Writing $\tilde{H} = \tilde{H}_o + \tilde{H}_{\rm int} = \int dx[H_0 + H_{\rm int}] = \int dx H$, the Hamiltonian can be written in the bosonic language as

$$H = H_0 + H_{\rm int} = \sum_{\alpha\sigma} v_F^{\alpha}(\nabla\Phi_{\alpha\sigma})^2 + \frac{1}{2\pi}\sum_{\alpha\alpha'} V_{\alpha\alpha'\alpha'\alpha}\sum_{\sigma\sigma'}\nabla\Phi_{\alpha\sigma}\nabla\Phi_{\alpha'\sigma'}, \tag{29}$$

where the sums over the α and σ indices include all the modes at both Dirac points. We further introduce bosons corresponding to different charge, spin sectors for different channels as follows:

$$\Phi_{\alpha c} = \frac{\Phi_{\alpha\uparrow} + \Phi_{\alpha\downarrow}}{\sqrt{2}}; \quad \Phi_{\alpha s} = \frac{\Phi_{\alpha\uparrow} - \Phi_{\alpha\downarrow}}{\sqrt{2}}, \tag{30}$$

where $\alpha = 1$ for uniformly driven SLG, $\alpha = 1, 2$ (boundary of uniformly driven BLG) or K and K' (interface of SLG) or $1_K, 2_K, 1_{K'}, 2_{K'}$ (interface of BLG) are different channels; here, c denotes the charge sector and s denotes the spin sector. Simplifying we get

$$\sum_{\sigma\sigma'}\nabla\Phi_{\alpha\sigma}\nabla\Phi_{\alpha'\sigma'} = 2\nabla\Phi_{\alpha c}\nabla\Phi_{\alpha' c}. \tag{31}$$

So the Hamiltonian can be written in terms of the charge and spin bosons as

$$H_0 = \sum_{\alpha} v_F^{\alpha}[(\nabla\Phi_{\alpha c})^2 + (\nabla\Phi_{\alpha s})^2], \tag{32}$$

$$H_{\rm int} = \frac{1}{\pi}\sum_{\alpha\alpha'} V_{\alpha\alpha'\alpha'\alpha}\nabla\Phi_{\alpha c}\nabla\Phi_{\alpha' c}, \tag{33}$$

where we note that the Coulomb interaction term modifies only the charge sector. Thus, in the absence of scatterings involving spin, the SU(2) spin symmetry is intact and the spin sector is not expected to be renormalized.

A. Uniformly irradiated SLG

In the case of uniformly irradiated SLG, there is a single charge mode, which decouples itself from the spin mode, following our previous discussion. The Hamiltonian of the charge mode is simply then

$$H_c = (\nabla\Phi_c)^2 \times \left(v_F + \frac{1}{\pi}V\right) \equiv \Lambda(\nabla\Phi_c)^2, \tag{34}$$

where V is the forward scattering amplitude, which simply implies a renormalized Fermi velocity of $\Lambda = (v_F + \frac{1}{\pi}V)$.

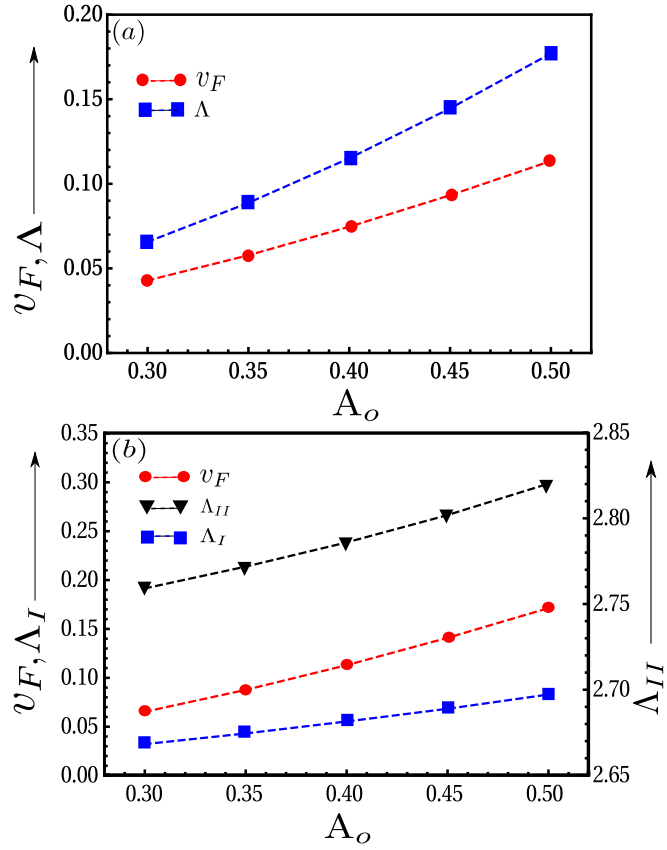

FIG. 5. (a) The renormalized velocity of the charge sector, Λ of the edge modes at the boundary of uniformly driven SLG, under Coulomb interaction, as a function of the driving amplitude A_0. (b) The renormalized velocities, Λ_I and Λ_{II} of the edge modes at the boundary of uniformly driven BLG, under Coulomb interaction as a function of the driving amplitude A_0. The velocities before the introduction of the Coulomb interaction are $v_F^1 \approx v_F^2 = v_F$ are also shown in both the graphs. The velocities are measured in units of $v = 3ta_0/2\hbar$.

The correlation functions of the fermions, which are the same for both $\sigma = \{\uparrow\downarrow\}$ spins, are given by [51,52]

$$\langle\hat{\Psi}_\sigma(y,t)\hat{\Psi}^{\dagger}_\sigma(0,0)\rangle \sim \exp(\langle\Phi_\sigma(y,t)\Phi^{\dagger}_\sigma(0,0)\rangle) \tag{35}$$

$$\text{with} \quad \Phi_{\{\uparrow\downarrow\}} = \frac{\Phi_c \pm \Phi_s}{\sqrt{2}}.$$

If v_i is the velocity of ith diagonal mode ($i = c, s$), one can further write

$$\langle\Phi_i(y,t)\Phi_j(0,0)\rangle = -\frac{1}{4\pi}\ln(y - v_i t)\delta_{ij}, \tag{36}$$

which gives us

$$\langle\hat{\Psi}_\sigma(y,t)\hat{\Psi}^{\dagger}_\sigma(0,0)\rangle \sim \frac{1}{(y-\Lambda t)^{\frac{1}{2}}}\frac{1}{(y - v_F t)^{\frac{1}{2}}}. \tag{37}$$

We show the variation of Λ as a function of the driving amplitude in Fig. 5(a).

B. Uniformly irradiated BLG and interface at SLG

The Hamiltonian for the charge sector, when there are two edge modes, either at the boundary of a uniformly irradiated

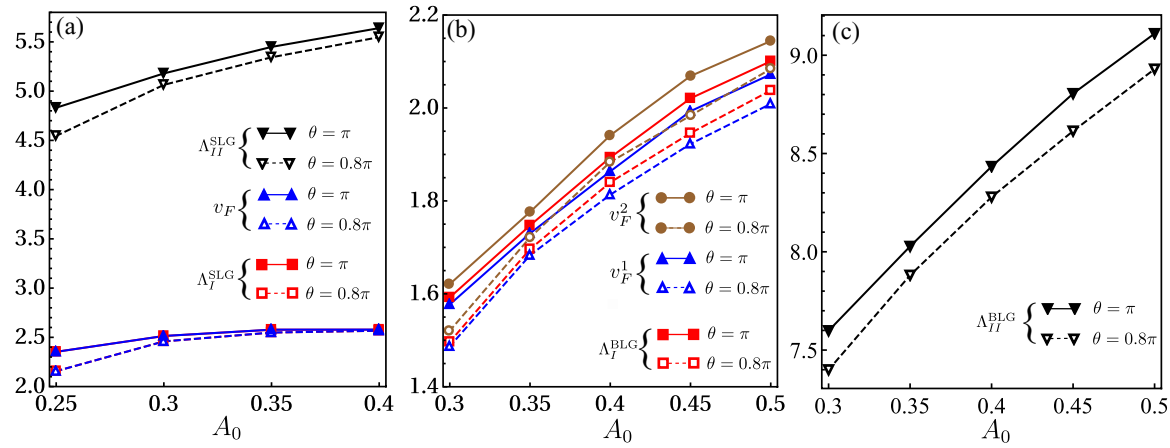

FIG. 6. The renormalized velocities of the edge modes, at the interface of regions driven with opposite polarizations, under Coulomb interaction as a function of the driving amplitude A_0 and the difference (θ) of the polarization angle of the irradiation between the left and right halves of the nanoribbon as shown in Fig. 1. $\theta=\pi$ represents the maximum difference—the case where the two drives are right and left circularly polarized. In (a), we show the two renormalized velocities Λ_I^{SLG} and Λ_{II}^{SLG} for the edge modes of the SLG setup. Here, v_F is the velocity of the two original modes. Similarly in (b) and (c) we show the result for the BLG system, where only the two modes of the (+) sector are renormalized (see the main text), with renormalized velocities Λ_I^{BLG} and Λ_{II}^{BLG}. The velocities are measured in units of $v=3ta_0/2\hbar$.

BLG or at the interface of oppositely polarized irradiation on SLG, can be written as

$$H_c=[\nabla\Phi_{1c}\quad\nabla\Phi_{2c}]R\begin{bmatrix}\nabla\Phi_{1c}\\ \nabla\Phi_{2c}\end{bmatrix},$$
$$R=\begin{bmatrix}v_F^1+\frac{1}{\pi}V_A & \frac{1}{\pi}V_B\\ \frac{1}{\pi}V_B & v_F^2+\frac{1}{\pi}V_A\end{bmatrix}, \tag{38}$$

where we have explicitly used the form of the resulting scattering matrix. $v_F^{1/2}$ are the Fermi velocities of the noninteracting edge modes (1/2 correspond to K/K' for the case of interface states at SLG). Here $V_A=V_{\alpha\alpha\alpha\alpha}$ and $V_B=V_{\alpha\alpha'\alpha'\alpha}$ ($\alpha\neq\alpha'$) as well as the Fermi velocities depend on specific parameters and the system in consideration (such as whether it is at the edge of uniformly irradiated BLG or at the interface of differently irradiated regions at the SLG, as well as the nature of the edge). This sector can then be diagonalized using the canonical transformation

$$\Phi_{Kc}=\cos\Theta_s\tilde{\Phi}_{1c}+\sin\Theta_s\tilde{\Phi}_{2c},$$
$$\Phi_{K'c}=-\sin\Theta_s\tilde{\Phi}_{1c}+\cos\Theta_s\tilde{\Phi}_{2c}, \tag{39}$$

with $\tan(2\Theta_s)=\frac{2}{\pi}V_B/(v_F^2-v_F^1)$. If $V_B\neq 0$ and $v_F^1\approx v_F^2$, one obtains $\Theta_s\approx\pi/4$, whereas if $V_B=0$, then $\Theta_s=0$. The renormalized velocities become

$$\Lambda_I=R_{11}\cos^2\Theta_s+R_{22}\sin^2\Theta_s-2R_{12}\sin\Theta_s\cos\Theta_s, \tag{40}$$

$$\Lambda_{II}=R_{11}\sin^2\Theta_s+R_{22}\cos^2\Theta_s+2R_{12}\sin\Theta_s\cos\Theta_s. \tag{41}$$

In Fig. 5(b), we show the renormalized velocities Λ_I and Λ_{II} as a function of the strength of the incident radiation for the edge modes of uniformly irradiated BLG. In Fig. 6(b), we also show the corresponding renormalized velocities for the modes at the interface at SLG, where we also study two possible differences of the polarization angle (θ): $\theta=\pi$ where the left and right halves of the graphene layer are irradiated with left and right circularly polarized light and for $\theta=0.8\pi$ where the polarization difference is slightly less. Interestingly, we find that the velocities are strongly renormalized, in either case, as a function of the amplitude of the light. They also depend on the difference in polarization of light impinging on the two halves of the SLG.

We next compute the correlation functions, following the discussion in the previous section. The correlation function of the original modes (1,2) are given by

$$\langle\hat{\Psi}_{1\sigma}(y,t)\hat{\Psi}_{1\sigma}^{\dagger}(0,0)\rangle \sim\frac{1}{(y-\Lambda_I t)^{\frac{\cos^2\Theta_s}{2}}}\frac{1}{(y-\Lambda_{II}t)^{\frac{\sin^2\Theta_s}{2}}}\frac{1}{(y-v_F t)^{\frac{1}{2}}}, \tag{42}$$

$$\langle\hat{\Psi}_{2\sigma}(y,t)\hat{\Psi}_{2\sigma}^{\dagger}(0,0)\rangle \sim\frac{1}{(y-\Lambda_I t)^{\frac{\sin^2\Theta_s}{2}}}\frac{1}{(y-\Lambda_{II}t)^{\frac{\cos^2\Theta_s}{2}}}\frac{1}{(y-v_F t)^{\frac{1}{2}}}. \tag{43}$$

We obtain $\Theta_s\approx\pi/4$ (thus, $\sin^2\Theta_s\approx\cos^2\Theta_s\approx 1/\sqrt{2}$) for the relevant parameters, with weak dependence on the amplitude of the driving and the polarization angle (not shown). It is easy to check that, if one turns off the interaction, the correlation functions become each of a fermionic mode with velocities $v_F=v_F^1\approx v_F^2$. Finally, for a uniformly driven arm-chair nanoribbon of bilayer graphene, the results of velocity renormalization of the edge modes are discussed in Appendix C.

C. Interface modes of BLG

For the case of BLG, one can proceed similar to the SLG case. We start by writing the charge sector as

$$H^c\equiv\sum_{\alpha}Q^o_{\alpha\alpha}\nabla\Phi_{\alpha c}\nabla\Phi_{\alpha c}+\sum_{\alpha\alpha'}Q_{\alpha\alpha'}\nabla\Phi_{\alpha c}\nabla\Phi_{\alpha' c}, \tag{44}$$

where

$$Q^o=\begin{bmatrix} v_F^1 & 0 & 0 & 0\\ 0 & v_F^2 & 0 & 0\\ 0 & 0 & v_F^1 & 0\\ 0 & 0 & 0 & v_F^2\end{bmatrix};\ Q=\begin{bmatrix} P & P\\ P & P\end{bmatrix};\ P=\frac{1}{\pi}\begin{bmatrix} V_A & V_B\\ V_B & V_A\end{bmatrix}, \tag{45}$$

where $v_F^{1_K}\approx v_F^{1_{K'}}=v_F^1$ and $v_F^{2_K}\approx v_F^{2_{K'}}=v_F^2$. The form of the Q and P matrices arises from the computation of the scattering matrix elements. We proceed by performing another transformation

$$\Phi^+_{\eta c}=\frac{\Phi_{\eta_K c}+\Phi_{\eta_{K'} c}}{\sqrt{2}};\quad \Phi^-_{\eta c}=\frac{\Phi_{\eta_K c}-\Phi_{\eta_{K'} c}}{\sqrt{2}}, \tag{46}$$

where $\eta=1,2$, to write

$$H^c=\sum_\eta v_F^\eta[(\nabla\Phi^+_{\eta c})^2+(\nabla\Phi^-_\eta)^2]+\frac{2}{\pi}\sum_{\eta\eta'}V_{\eta\eta'\eta'\eta}(\nabla\Phi^+_{\eta c}\nabla\Phi^+_{\eta' c}), \tag{47}$$

$$H^c_+=\sum_\eta v_F^\eta[(\nabla\Phi^+_{\eta c})^2]+\frac{2}{\pi}\sum_{\eta\eta'}V_{\eta\eta'\eta'\eta}(\nabla\Phi^+_{\eta c}\nabla\Phi^+_{\eta' c}), \tag{48}$$

$$H^c_-=\sum_\eta v_F^\eta[(\nabla\Phi^-_{\eta c})^2], \tag{49}$$

allowing us to further write the (+) sector as

$$H^+_c=[\nabla\Phi^+_{1c}\quad\nabla\Phi^+_{2c}]R^{\rm BLG}\begin{bmatrix}\nabla\Phi^+_{1c}\\ \nabla\Phi^+_{2c}\end{bmatrix},$$
$$R^{\rm BLG}=\begin{bmatrix} v_F^1+\frac{2}{\pi}V_A & \frac{2}{\pi}V_B\\ \frac{2}{\pi}V_B & v_F^2+\frac{2}{\pi}V_A,\end{bmatrix} \tag{50}$$

where it is evident that only the (+) modes are renormalized. This sector can then be diagonalized using the canonical transformation

$$\Phi^+_{1c}=\cos\Theta_b\tilde\Phi_{1c}+\sin\Theta_b\tilde\Phi_{2c},$$
$$\Phi^+_{2c}=-\sin\Theta_b\tilde\Phi_{1c}+\cos\Theta_b\tilde\Phi_{2c}, \tag{51}$$

with $\tan(2\Theta_b)=\frac{4}{\pi}V_B/(v_F^2-v_F^1)$. For $V_B\neq 0$ and $v_F^1\approx v_F^2$, we obtain $\Theta_b\approx\pi/4$, whereas if $V_B=0$, then $\Theta_b=0$. The renormalized velocities of the (+) sector become

$$\Lambda_I^{\rm BLG}=R_{11}^{\rm BLG}\cos^2\Theta_b+R_{22}^{\rm BLG}\sin^2\Theta_b-2R_{12}^{\rm BLG}\sin\Theta_b\cos\Theta_b, \tag{52}$$

$$\Lambda_{II}^{\rm BLG}=R_{11}^{\rm BLG}\sin^2\Theta_b+R_{22}^{\rm BLG}\cos^2\Theta_b+2R_{12}\sin\Theta_b\cos\Theta_b, \tag{53}$$

whereas, for the (−) sector, the modes remain unrenormalized. In Fig. 5, we show the renormalized velocities $\Lambda_I^{\rm BLG}$ and $\Lambda_{II}^{\rm BLG}$ as a function of the strength of the incident radiation, as well as for two values of the polarization angle (θ), which show strong renormalization.

In terms of these diagonalized fields, the fields of the original bosonic operator can be written as

$$\Phi_{1_K c}=\frac{1}{\sqrt{2}}[\cos\Theta\tilde\Phi_{1c}+\sin\Theta\tilde\Phi_{2c}+\Phi^-_{1c}],$$
$$\Phi_{2_K c}=\frac{1}{\sqrt{2}}[-\sin\Theta\tilde\Phi_{1c}+\cos\Theta\tilde\Phi_{2c}+\Phi^-_{2c}],$$
$$\Phi_{1_{K'} c}=\frac{1}{\sqrt{2}}[\cos\Theta\tilde\Phi_{1c}+\sin\Theta\tilde\Phi_{2c}-\Phi^-_{1c}],$$
$$\Phi_{2_{K'} c}=\frac{1}{\sqrt{2}}[-\sin\Theta\tilde\Phi_{1c}+\cos\Theta\tilde\Phi_{2c}-\Phi^-_{2c}],$$
$$\Phi_{g\{\uparrow\downarrow\}}=\frac{\Phi_{gc}\pm\Phi_{gs}}{\sqrt{2}};\quad g=\{1_K,1_{K'},2_K,2_{K'}\}. \tag{54}$$

Similar to the case of single-layer graphene, the correlation functions are then given by

$$\langle\hat\Psi_{1_{(K,K')\sigma}}(y,t)\hat\Psi^\dagger_{1_{(K,K')\sigma}}(0,0)\rangle\sim\frac{1}{\left(y-\Lambda_I^{\rm BLG}t\right)^{\frac{\cos^2\Theta_b}{4}}}\times\frac{1}{\left(y-\Lambda_{II}^{\rm BLG}t\right)^{\frac{\sin^2\Theta_b}{4}}}\frac{1}{\left(y-v_F^1t\right)^{\frac{3}{4}}} \tag{55}$$

and

$$\langle\hat\Psi_{2_{(K,K')\sigma}}(y,t)\hat\Psi^\dagger_{2_{(K,K')\sigma}}(0,0)\rangle\sim\frac{1}{\left(y-\Lambda_I^{\rm BLG}t\right)^{\frac{\sin^2\Theta_b}{4}}}\times\frac{1}{\left(y-\Lambda_{II}^{\rm BLG}t\right)^{\frac{\cos^2\Theta_b}{4}}}\frac{1}{\left(y-v_F^2t\right)^{\frac{3}{4}}}. \tag{56}$$

We obtain $\Theta_b\approx\pi/4$ (thus, $\sin^2\Theta_b\approx\cos^2\Theta_b\approx 1/\sqrt{2}$) for the relevant parameters, with a weak dependence on the amplitude of the driving and the polarization angle (not shown). Similar to the case of SLG. it is easy to check that, if we turn off the interaction, the correlation functions become each of a fermionic mode with velocities v_F^1 or v_F^2.

V. SUMMARY

For experimental realization, the crucial requirements are that the topological mass gap, $m=\lambda^2\gamma/\omega$ be larger than the temperature scale and the driving frequency be larger than the other energy scales. The intensity of the circularly polarized drive ($I=\frac{1}{2}c\epsilon_0E^2$) can be written as $I\approx 10^{14}\alpha_d^2(\hbar\omega/t)$ W/cm^2, where the unitless parameter $\alpha_d=eAa_0/\hbar$ characterizes the driving amplitude. Assuming the topological mass to be of the order of meV and the driving frequency to be order of an electron volt, we obtain $\alpha_d\sim 10^{-2}$, which in turn determines the required intensity of the drive. In an experimental setup, the possibility of heating may also need more careful consideration.

To summarize, we have studied the possibility of tunable chiral Luttinger liquid states at the interface of driven, topologically distinct states in two dimensions, specifically focusing on single and bilayer graphene systems. The nature of the gap opening of the bulk allows us to consider the effective interaction among the electrons at the topological steady states to be effectively time-independent so that we can apply standard bosonization techniques to these interacting

steady states. Our results suggest that these systems can act as a platform for highly tunable chiral Luttinger liquids, which can be further studied experimentally.

ACKNOWLEDGMENTS

The research of A.K. was supported by funding from SERB, DST (Goverment of India), MHRD (Goverment of India) and DAE (Goverment of India). SB acknowledges support from UGC (Goverment of India). We also acknowledge HPC fecility of IIT Kanpur for computational work. T.M. acknowledges discussions with A. Dutta and the support of SERB, DST (Goverment of India)

APPENDIX A

In this Appendix, we write the van Vleck expansion up to second order for bilayer graphene, which gives rise to a small difference between the velocities v_1 and v_2 of the topological edge modes at K and K' momentum points. The second order, i.e., $\mathcal{O}(\omega^{-2})$ correction to $H_{\rm eff}$, under the van Vleck high-frequency expansion, is given by

$$\frac{1}{2\omega^2}\sum_{n=1}^{\infty}\frac{1}{n^2}([[\mathcal{H}_n,\mathcal{H}_0],\mathcal{H}_{-n}]+\text{H.c.}).$$

In our case, due to the sine and cosine nature of the driving, $\mathcal{H}_{\pm1}$ are the only nonzero Fourier coefficients of the Hamiltonian and the resulting correction term reduces to calculating $([[\mathcal{H}_1,\mathcal{H}_0],\mathcal{H}_{-1}])/(2\omega^2)$. For convenience of notation, we introduce the following: $\alpha = A_x + A_y e^{-i\theta}$, $\beta = A_x - A_y e^{i\theta}$, $\Gamma = A_x + A_y e^{i\theta}$, and $\delta = A_x - A_y e^{-i\theta}$. Further we use $C \equiv \frac{\lambda^2\gamma}{4\omega}\cos\theta$, $B \equiv 1 - \frac{\lambda^2}{4\omega^2}(\alpha\Gamma+\beta\delta)$, $D \equiv \frac{\lambda^2}{2\omega^2}\delta\Gamma$, and $E \equiv \frac{\lambda^2}{2\omega^2}\alpha\beta$ to obtain

$$H_{\rm eff} = \begin{pmatrix} -C & v\pi^\dagger B + Ev\pi & 0 & t_pE \\ v\pi B + Dv\pi^\dagger & C & t_pB & 0 \\ 0 & t_pB & -C & v\pi^\dagger B + Ev\pi \\ t_pD & 0 & v\pi B + Dv\pi^\dagger & C \end{pmatrix}. \tag{A1}$$

It is useful here to note the relations $B = 1 - \frac{\lambda^2(A_x^2+A_y^2)}{2\omega^2}$ and $D^\dagger = E$.

Using this Hamiltonian we proceed to calculate the effective two-band low-energy sector. This can be done in the same way as was done in the main text [1] to have

$$H^L_{\rm eff} = \begin{pmatrix} (H^L_{\rm eff})_{1,1} & (H^L_{\rm eff})_{1,2} \\ (H^L_{\rm eff})_{2,1} & (H^L_{\rm eff})_{2,2} \end{pmatrix}, \tag{A2}$$

where the matrix elements are as follows:

$$(H^L_{\rm eff})_{1,1} = -C - \frac{Cv^2}{C^2+t_p^2B^2}((B^2+ED)\pi^\dagger\pi + BD(\pi^\dagger)^2 + EB\pi^2), \tag{A3}$$

$$(H^L_{\rm eff})_{1,2} = t_pE - \frac{t_pBv^2}{C^2+t_p^2B^2}(B^2(\pi^\dagger)^2 + E^2\pi^2 + 2EB\pi^\dagger\pi), \tag{A4}$$

$$(H^L_{\rm eff})_{2,1} = t_pD - \frac{t_pBv^2}{C^2+t_p^2B^2}(B^2\pi^2 + D^2(\pi^\dagger)^2 + 2BD\pi^\dagger\pi), \tag{A5}$$

$$(H^L_{\rm eff})_{2,2} = C + \frac{Cv^2}{C^2+t_p^2B^2}((B^2+ED)\pi^\dagger\pi + BD(\pi^\dagger)^2 + EB\pi^2). \tag{A6}$$

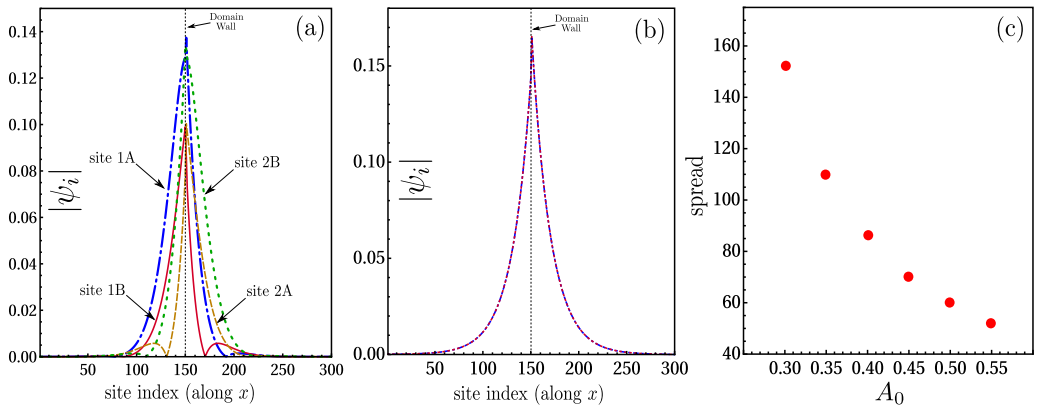

FIG. 7. The domain-wall state's wave function for (a) BLG and (b) SLG for a larger system size (1200 sites for BLG and 600 sites for SLG) and for the amplitude of the drive $A_0 = 0.5$ and $\omega/t = 30$, showing the confined nature of the state. (c) Plot of the standard deviation of the amplitude of the wave function, which we estimate as spread, as a function of the amplitude of the drive A_0 for the domain-wall state in SLG.

This is valid in the low-energy regime when $\epsilon \ll t_p(1-\frac{\lambda^2}{2\omega^2}(A_x^2+A_y^2))$, which holds if one ensures that $\frac{\lambda^2 A_x A_y}{\omega} \ll t_p(1-\frac{\lambda^2}{2\omega^2}(A_x^2+A_y^2))$. We can make some simplifications to the above elements of H^L_{eff} by making approximations where terms of $\mathcal{O}(\omega^{-4})$ are dropped. Under these approximations are, $(B^2+ED) \approx 1-\frac{\lambda^2}{2\omega^2}(A_x^2+A_y^2)$, $BD \approx D = \frac{\lambda^2}{2\omega^2}\delta\Gamma$, $EB \approx E = \frac{\lambda^2}{2\omega^2}\alpha\beta$ and $E^2 = D^2 = 0$. Additionally, given the condition for the low-energy regime it follows that $t_p^2 B^2 \gg C^2$. Using them, we re-examine the of-diagonal terms of H^L_{eff},

$$\left(H^L_{\text{eff}}\right)_{1,2} \approx t_p E - \frac{v^2}{t_p B}(B^2(\pi^\dagger)^2 + 2E\pi^\dagger\pi), \tag{A7}$$

$$\left(H^L_{\text{eff}}\right)_{2,1} \approx t_p D - \frac{v^2}{t_p B}(B^2\pi^2 + 2D\pi^\dagger\pi). \tag{A8}$$

By comparing the above off-diagonal terms to the off-diagonal terms for the low-energy effective Hamiltonian computed in Eq. (11) where only the $\mathcal{O}(\omega^{-1})$ correction from the driving had been included, we see that the modifications coming from the t_pD and t_pE kind of terms here, as higher-order driving effects, are responsible for the observed asymmetry of the Fermi velocities of the chiral Luttinger edge modes in this system. Thus higher-order terms in the van Vleck expansion are significant in the regime where edge modes are observed under the application of driving and are a manifestation of the long range hoppings induced by the drive.

APPENDIX B

The spread of the wave function of the edge or domain-wall mode depends on the amplitude and the frequency of the drive. In Fig. 7, we show explicitly the spread of the wave function using a larger system size for numerical simulation as well as how the spread changes with increasing amplitude of drive A_0.

APPENDIX C

In this Appendix, we discuss uniformly irradiated armchair nanoribbons. We have shown the Luttinger liquid analysis for uniformly irradiated BLG sample in Eqs. (38)–(42) and have presented the results for zigzag edge SLG sample in Fig. 2, 3, and 5. We are not showing the same analysis in the context of a BLG nanoribbon with armchair edge. Here, we only show the numerical results as presented in Fig. 8.

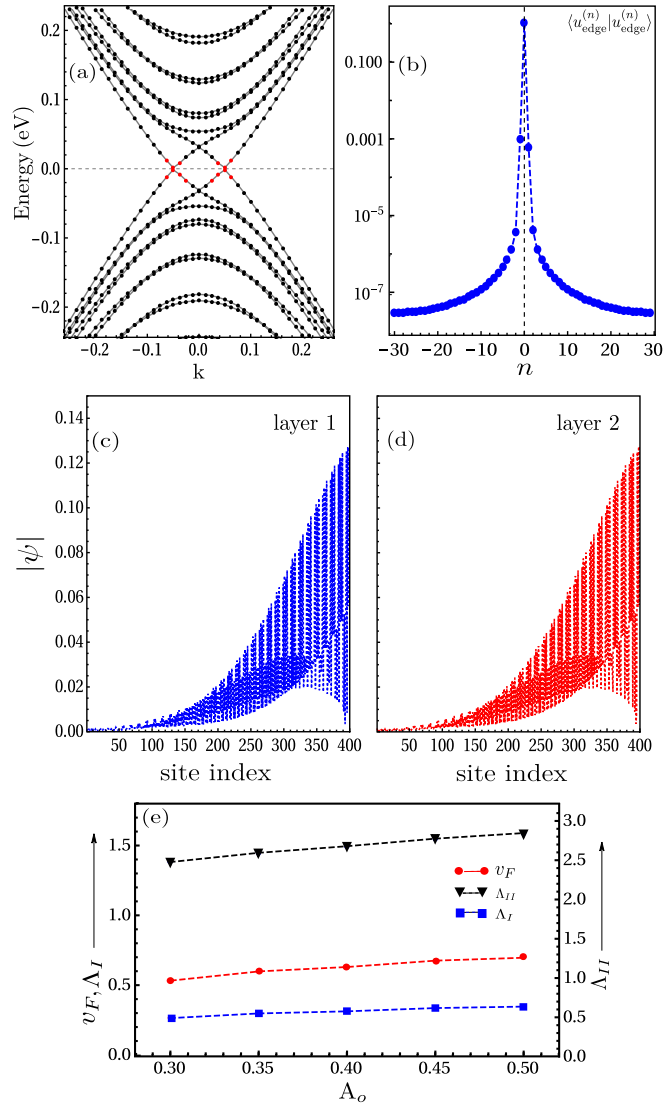

FIG. 8. Bilayer graphene nanoribbon with armchair edges. (a) The spectrum, highlighting the edge modes; (b) the Fourier components of the Floquet states; [(c) and (d)] the spread of the wave function of the edge modes; and (e) renormalized velocities Λ_I and Λ_{II} of the edge modes for the driven system. All other parameters are the same as in the Fig. 3.

[1] E. McCann and V. I. Fal'ko, Phys. Rev. Lett. **96**, 086805 (2006).

[2] E. V. Castro, K. S. Novoselov, S. V. Morozov, N. M. R. Peres, J. M. B. dos Santos, J. Nilsson, F. Guinea, A. K. Geim, and A. H. Castro Neto, Phys. Rev. Lett. **99**, 216802 (2007).

[3] J. B. Oostinga *et al.*, Nat. Mater. **7**, 151 (2008).

[4] Y. Zhang *et al.*, Nature (London) **459**, 820 (2009).

[5] For a review, see E. McCann and M. Koshino, Rep. Prog. Phys. **76**, 056503 (2013).

[6] A. H. Castro Neto, F. Guinea, N. M. R. Peres, K. S. Novoselov, and A. K. Geim, Rev. Mod. Phys. **81**, 109 (2009).

[7] I. Martin, Y. M. Blanter, and A. F. Morpurgo, Phys. Rev. Lett. **100**, 036804 (2008).

[8] A. J. Heeger, S. Kivelson, J. R. Schrieffer, and W. P. Su, Rev. Mod. Phys. **60**, 781 (1988).

[9] G. W. Semenoff, V. Semenoff, and F. Zhou, Phys. Rev. Lett. **101**, 087204 (2008).

[10] R. Jackiw and C. Rebbi, Phys. Rev. D **13**, 3398 (1976).

[11] M. Killi, T. C. Wei, I. Affleck, and A. Paramekanti, Phys. Rev. Lett. **104**, 216406 (2010).

[12] N. H. Lindner, G. Refael, and V. Galitski, Nat. Phys. **7**, 490 (2011).

[13] B. Dora, J. Cayssol, F. Simon, and R. Moessner, Phys. Rev. Lett. **108**, 056602 (2012).
[14] M. S. Rudner, N. H. Lindner, E. Berg, and M. Levin, Phys. Rev. X **3**, 031005 (2013).
[15] N. Goldman and J. Dalibard, Phys. Rev. X **4**, 031027 (2014).
[16] A. Farrell and T. Pereg-Barnea, Phys. Rev. B **93**, 045121 (2016).
[17] P. Titum, E. Berg, M. S. Rudner, G. Refael, and N. H. Lindner, Phys. Rev. X **6**, 021013 (2016).
[18] J. Klinovaja, P. Stano, and D. Loss, Phys. Rev. Lett. **116**, 176401 (2016).
[19] M. Rodriguez-Vega, A. Kumar, and B. Seradjeh, Phys. Rev. B **100**, 085138 (2019).
[20] T. Oka and H. Aoki, Phys. Rev. B **79**, 081406(R) (2009).
[21] T. Kitagawa, T. Oka, A. Brataas, L. Fu, and E. Demler, Phys. Rev. B **84**, 235108 (2011).
[22] A. Kundu, H. A. Fertig, and B. Seradjeh, Phys. Rev. Lett. **113**, 236803 (2014).
[23] G. Usaj, P. M. Perez-Piskunow, L. E. F. Foa Torres, and C. A. Balseiro, Phys. Rev. B **90**, 115423 (2014).
[24] A. Kundu, H. A. Fertig, and B. Seradjeh, Phys. Rev. Lett. **116**, 016802 (2016).
[25] T. Mikami, S. Kitamura, K. Yasuda, N. Tsuji, T. Oka, and H. Aoki, Phys. Rev. B **93**, 144307 (2016).
[26] P. Mohan, R. Saxena, A. Kundu, and S. Rao, Phys. Rev. B **94**, 235419 (2016).
[27] B. Mukherjee, P. Mohan, D. Sen, and K. Sengupta, Phys. Rev. B **97**, 205415 (2018).
[28] T. Mishra, A. Pallaprolu, T. Guha Sarkar, and J. N. Bandyopadhyay, Phys. Rev. B **97**, 085405 (2018).
[29] T. Mishra, T. G. Sarkar, and J. N. Bandyopadhyay, Eur. Phys. J. B **88**, 231 (2015).
[30] E. Suárez Morell and L. E. F. Foa Torres, Phys. Rev. B **86**, 125449 (2012).
[31] V. Dal Lago, E. Suárez Morell, and L. E. F. Foa Torres, Phys. Rev. B **96**, 235409 (2017).
[32] I. V. Iorsh, K. Dini, O. V. Kibis, and I. A. Shelykh, Phys. Rev. B **96**, 155432 (2017).
[33] P. Mohan and S. Rao, Phys. Rev. B **98**, 165406 (2018).
[34] J. W. McIver *et al.*, Nat. Phys. **16**, 38 (2020).
[35] E. Mostaani, N. D. Drummond, and V. I. Fal'ko, Phys. Rev. Lett. **115**, 115501 (2015).
[36] E. B. Fel'dman, Phys. Lett. A **104**, 479 (1984).
[37] E. S. Mananga and T. Charpentier, J. Chem. Phys. **135**, 044109 (2011).
[38] F. Casas, J. A. Oteo, and J. Ros, J. Phys. A: Math. Gen. **34**, 3379 (2001).
[39] T. Kuwahara, T. Mori, and K. Saito, Ann. Phys. **367**, 96 (2016).
[40] A. Eckardt and E. Anisimovas, New J. Phys. **17**, 093039 (2015).
[41] M. Bukov, L. D'Alessio, and A. Polkovnikov, Adv. Phys. **64**, 139 (2015).
[42] J. L. Mañes, F. Guinea, and M. A. H. Vozmediano, Phys. Rev. B **75**, 155424 (2007).
[43] S. Li, C.-C. Liu, and Y. Yao, New J. Phys. **20**, 033025 (2018).
[44] H. L. Calvo, L. E. F. Foa Torres, P. M. Perez-Piskunow, C. A. Balseiro, and G. Usaj, Phys. Rev. B **91**, 241404(R) (2015).
[45] D. A. Abanin, W. De Roeck, and F. Huveneers, Phys. Rev. Lett. **115**, 256803 (2015).
[46] T. Mori, T. Kuwahara, and K. Saito, Phys. Rev. Lett. **116**, 120401 (2016).
[47] D. A. Abanin, W. De Roeck, W. W. Ho, and F. Huveneers, Phys. Rev. B **95**, 014112 (2017).
[48] E. Kandelaki and M. S. Rudner, Phys. Rev. Lett. **121**, 036801 (2018).
[49] K. I. Seetharam, C.-E. Bardyn, N. H. Lindner, M. S. Rudner, and G. Refael, Phys. Rev. X **5**, 041050 (2015); K. I. Seetharam, C-E. Bardyn, N. H. Lindner, M. S. Rudner, and G. Refael, Phys. Rev. B **99**, 014307 (2019).
[50] M. Bukov and M. Heyl, Phys. Rev. B **86**, 054304 (2012).
[51] E. Fradkin, *Field Theories of Condensed Matter Physics* (Cambridge University Press, Cambridge, 2013).
[52] S. Rao and D. Sen, *Field Theories in Condensed Matter Physics*, Texts and Readings in Physical Sciences (Hindustan Book Agency, Gurgaon, 2001).